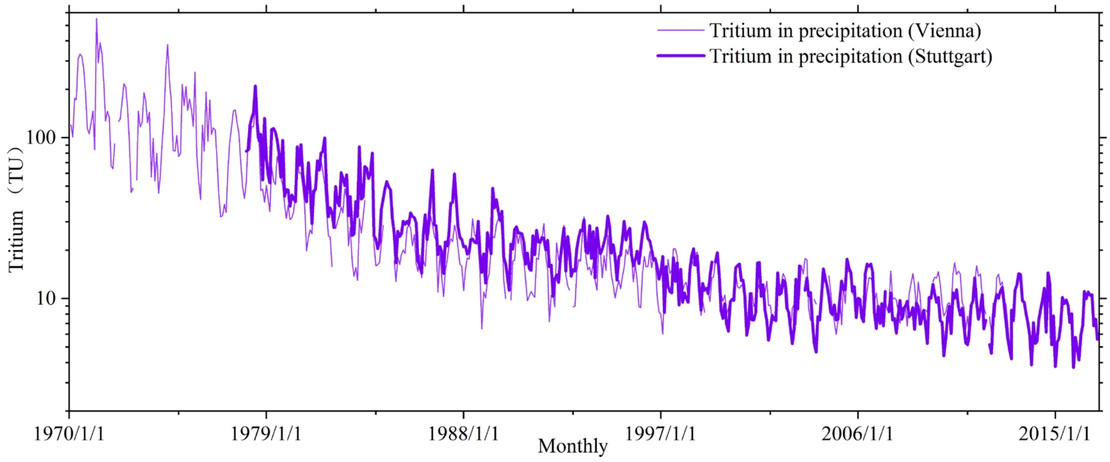

Figure S1. Long term ^{3}H data in precipitation at Vienna station and Stuttgart (thin violet line for Vienna station and dark violet line for Stuttgart station).

We estimated the sine wave parameters a_P, b_P and φ_P in each of the four precipitation zones (P1 – P4) based on the multiple regression coefficients reported by Allan et al. (2018) in which the study area is very closed to our catchment as follows:

$$a_P = (-7.90 * 10^{-6}) * La_P + (-2.62 * 10^{-6}) * Lo_P + 0.0006 * H_P + 0.28 * Tr_P - 0.009 * P_P - 0.43 \quad (S1)$$

$$\varphi_P = (-6.29 * 10^{-7}) * La_P + 1.82 \quad (S2)$$

$$b_P = (3.45 * 10^{-6}) * La_P + (1.19 * 10^{-6}) * Lo_P - 0.002 * H_P - 0.18 * Tr_P - 5.83 \quad (S3)$$

With La_P [°] latitude, Lo_P [°] longitude, H_P [m] elevation, Tr_P [°C] mean annual range of monthly temperatures, and P_P [cm] mean annual precipitation. Note that all of the above individual spatial predictor variables, averaged for each precipitation zone (P1 – P4) (Table S1).

Table S1 The sine parameters' predictor variables in different precipitation zones in the Neckar river basin.

Precipitation zone	La_P [°]	Lo_P [°]	Hp [m]	TrP [°C]	P_P [cm]
P1	48.42	8.87	568.04	19.90	93.28
P2	48.92	9.12	322.20	20.05	80.87
P3	49.05	9.71	420.53	20.09	88.97
P4	48.56	8.52	673.21	19.76	105.27
Stuttgart station	48.83	9.20	314.00	20.04	69.08

Table S2 The estimates of sine parameters for different precipitation zones and Stuttgart station.

	a_P [‰]	φ_P [rad]	b_P [‰]
P1	4.64	1.82	-10.55
P2	4.65	1.82	-10.08
P3	4.65	1.82	-10.29
P4	4.56	1.82	-10.73
Stuttgart	4.75	1.82	-10.06

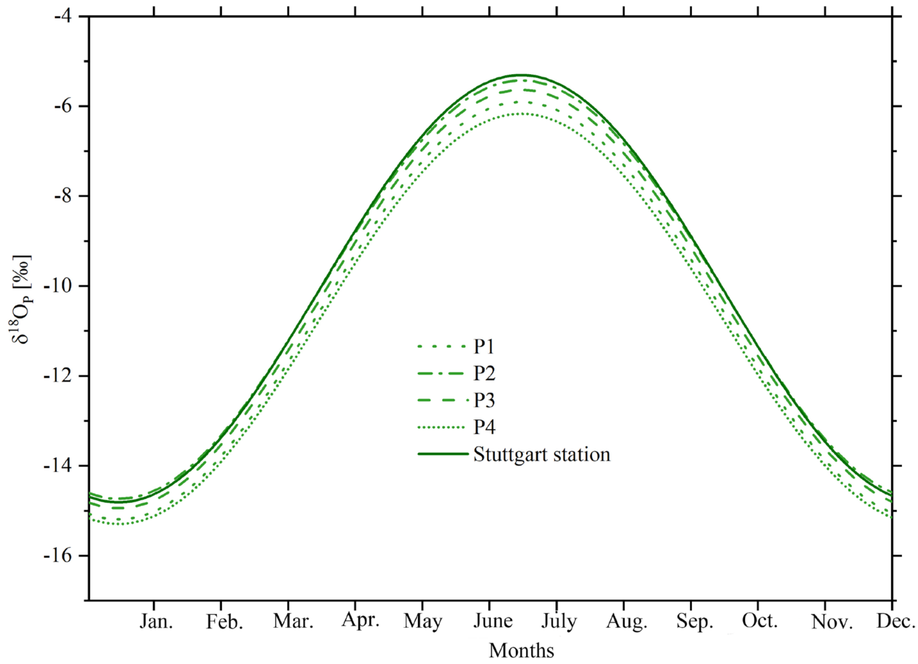

Figure S2. The $\delta^{18}O_P$ sine wave for precipitation zones (P1 – P4) and Stuttgart station.

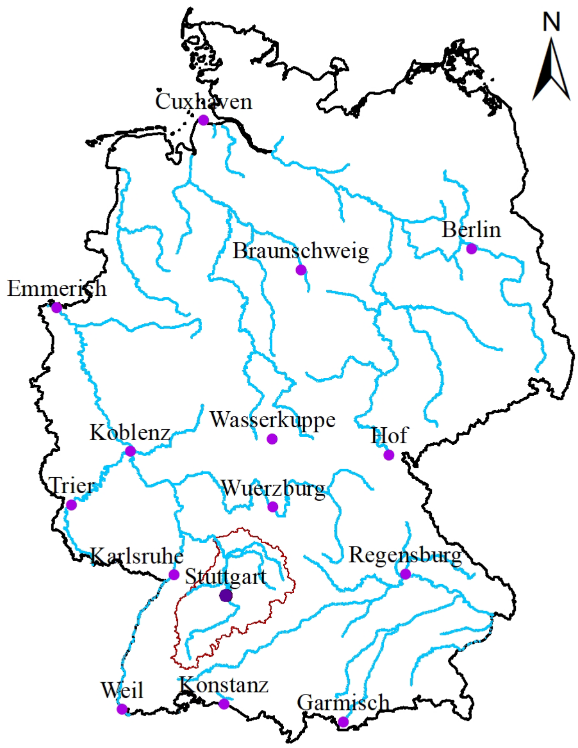

Figure S3. ^{3}H concentrations in precipitation observed at 15 multiple locations across Germany.

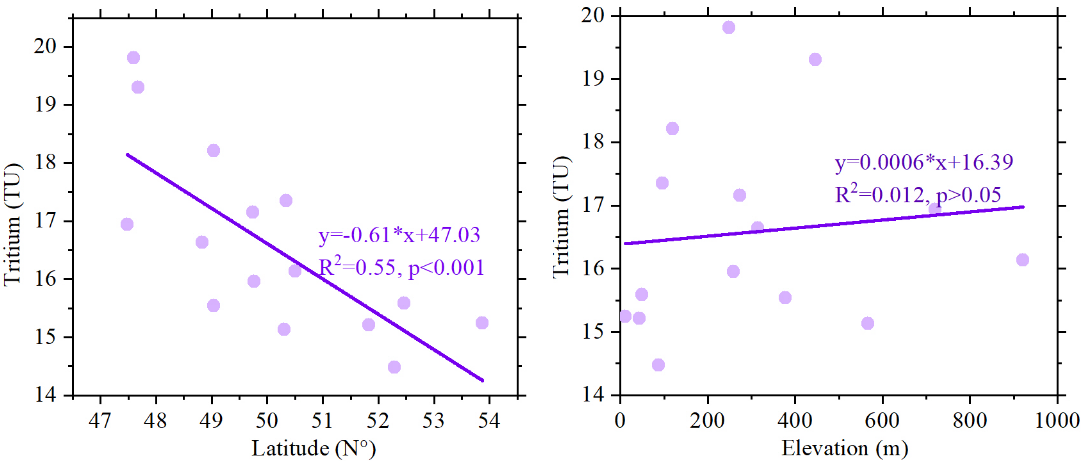

Figure S4. The linear regression relationships between ^3H concentrations in precipitation observed at 15 locations across Germany with latitude and elevation respectively.

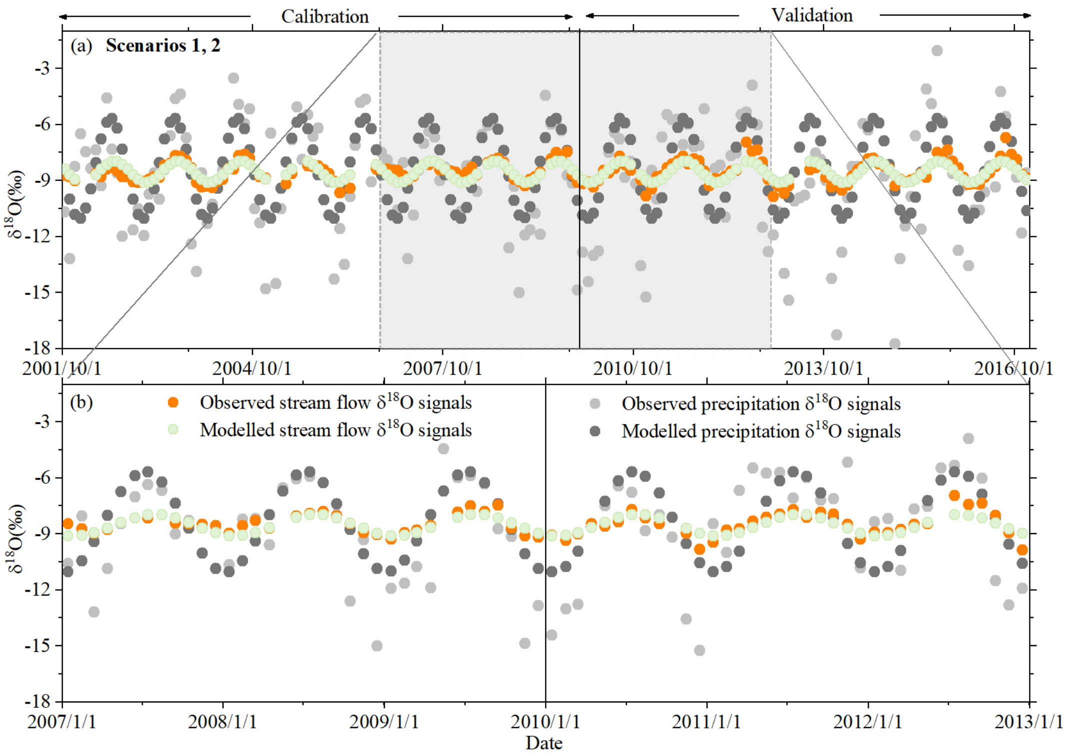

Figure S5. The time series of stream $\delta^{18}O$ reproduced by SW models, i.e., calibration strategy C_x (scenario 1, 2), for the model calibration and evaluation periods. (a) Observed $\delta^{18}O$ signals in precipitation (light grey dots) and modelled $\delta^{18}O$ signals in precipitation (dark grey dots), and observed stream $\delta^{18}O$signals (orange dots) as well as modelled stream $\delta^{18}O$signals (light green dots), (b) zoom-in of observed and modelled $\delta^{18}O$ signals for the 01/01/2007 – 31/12/2012 period.

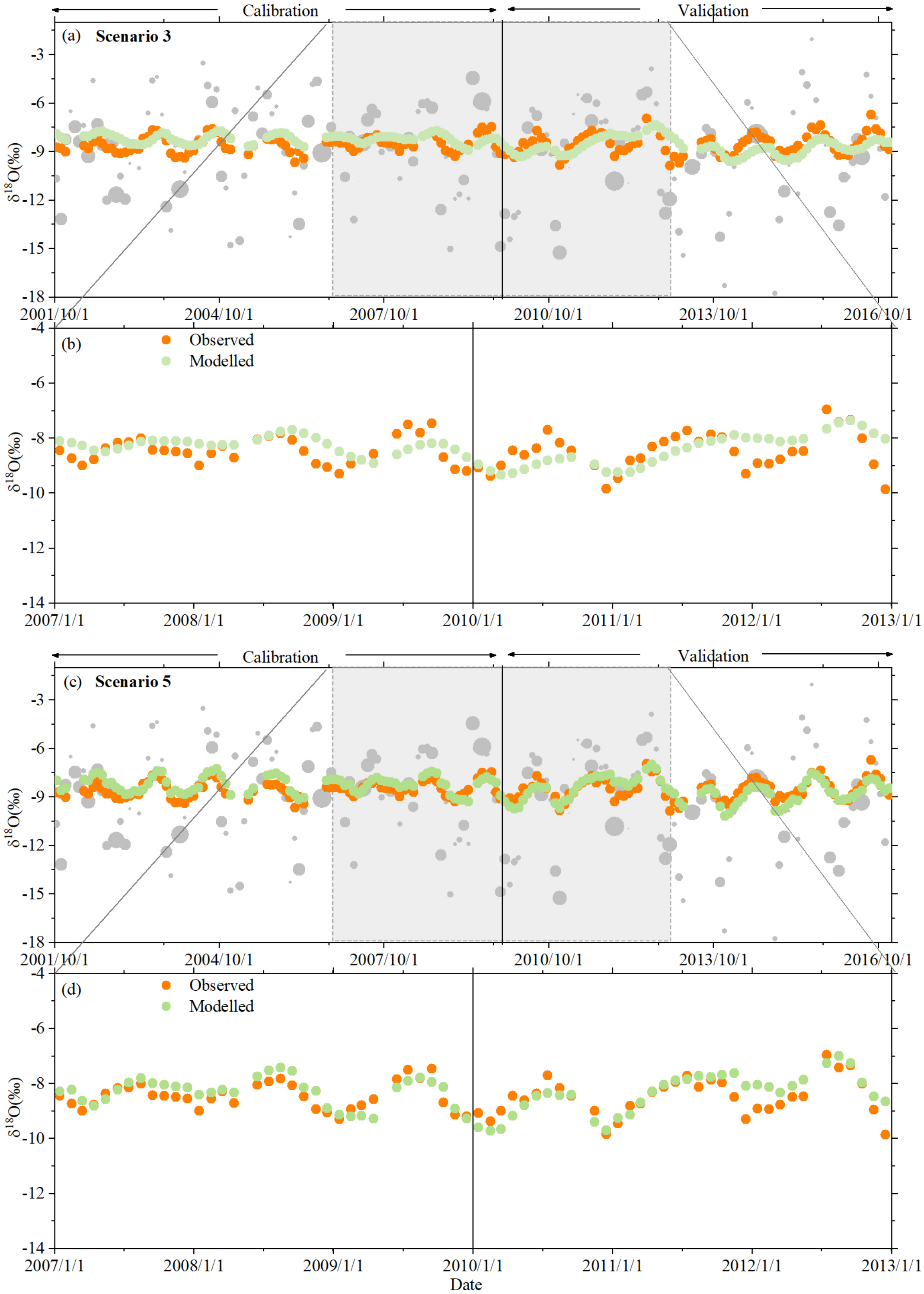

Figure S6. The time series of stream $\delta^{18}O$ reproduced by CO models, i.e., calibration strategy $C_{\delta^{18}O}$ (scenario3, 5), for the model calibration and evaluation periods. (a) Observed $\delta^{18}O$signals in precipitation (light grey dots; size of dots indicates the precipitation volume) and observed stream $\delta^{18}O$signals (orange dots) as well as the modelled stream $\delta^{18}O$signals (light green dots) for scenarios 3, (b) zoom-in of observed and modelled $\delta^{18}O$ signals in the stream for the 01/01/2007 – 31/12/2012 period for scenarios 3, (c) Observed $\delta^{18}O$signals in precipitation and in stream same as (a), and the modelled stream $\delta^{18}O$signals (relatively darker green dots) for scenarios 5, (d) zoom-in of observed and modelled $\delta^{18}O$ signals in the stream for the 01/01/2007 – 31/12/2012 period for scenarios 5.

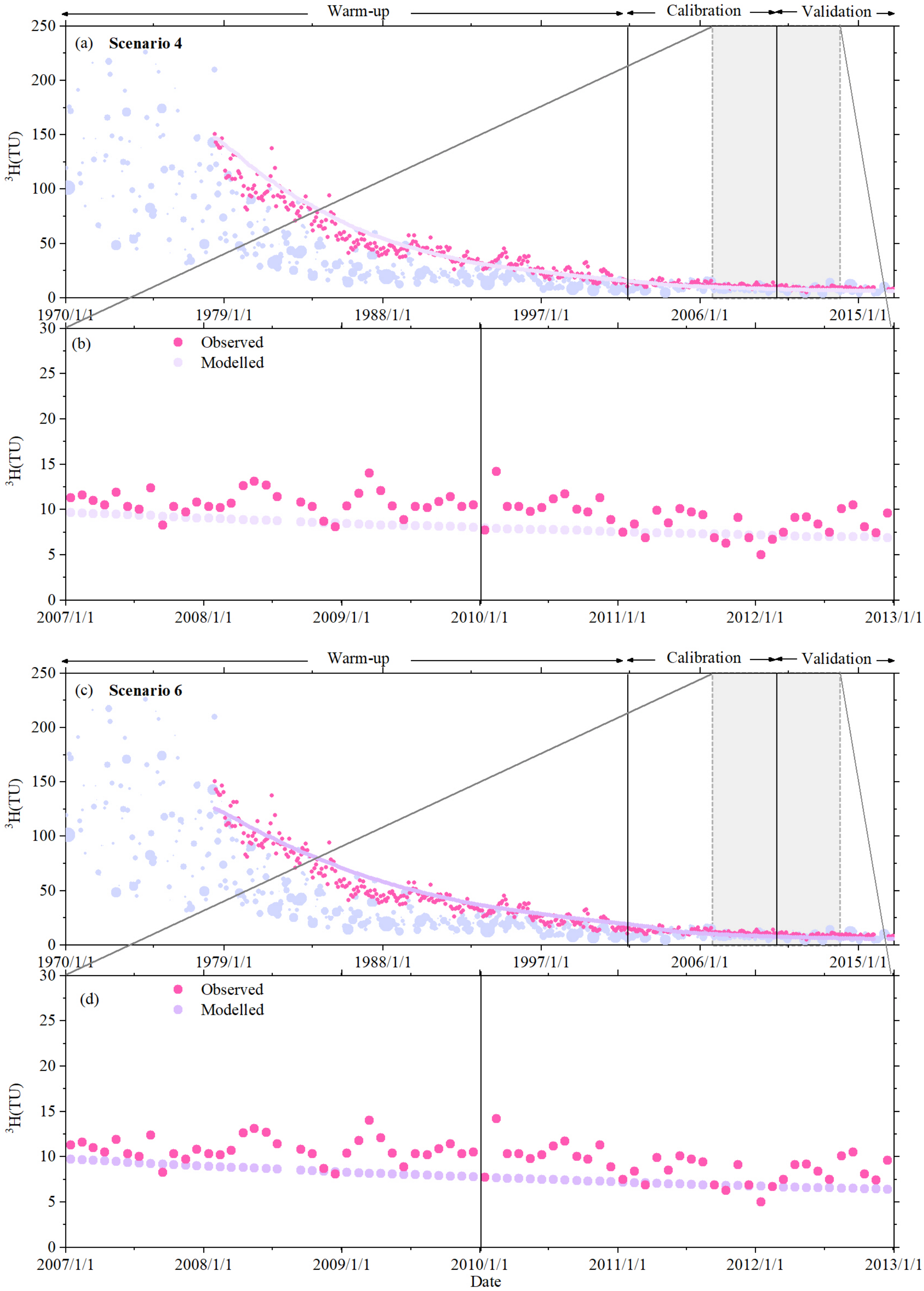

Figure S7. Time series of stream ^{3}H reproduced by CO models, i.e., calibration strategy $C_{^3H}$ (scenario4, 6), for the model calibration and evaluation periods. (a) Observed ^{3}H signals in precipitation (light blue-purple dots; size of dots indicates associated precipitation volume) and in streamflow (pink dots) as well as the modelled ^{3}H stream signal (light purple dots), (b) zoom-in of observed and modelled ^{3}H signals for the 01/01/2007 – 31/12/2012 period for scenarios 4, (c) Observed ^{3}H signals in precipitation and in stream same as (a), and the modelled stream ^{3}H signals (relatively darker purple dots) for scenarios 6, (d) zoom-in of observed and modelled ^{3}H signals in the stream for the 01/01/2007 – 31/12/2012 period for scenarios 6.

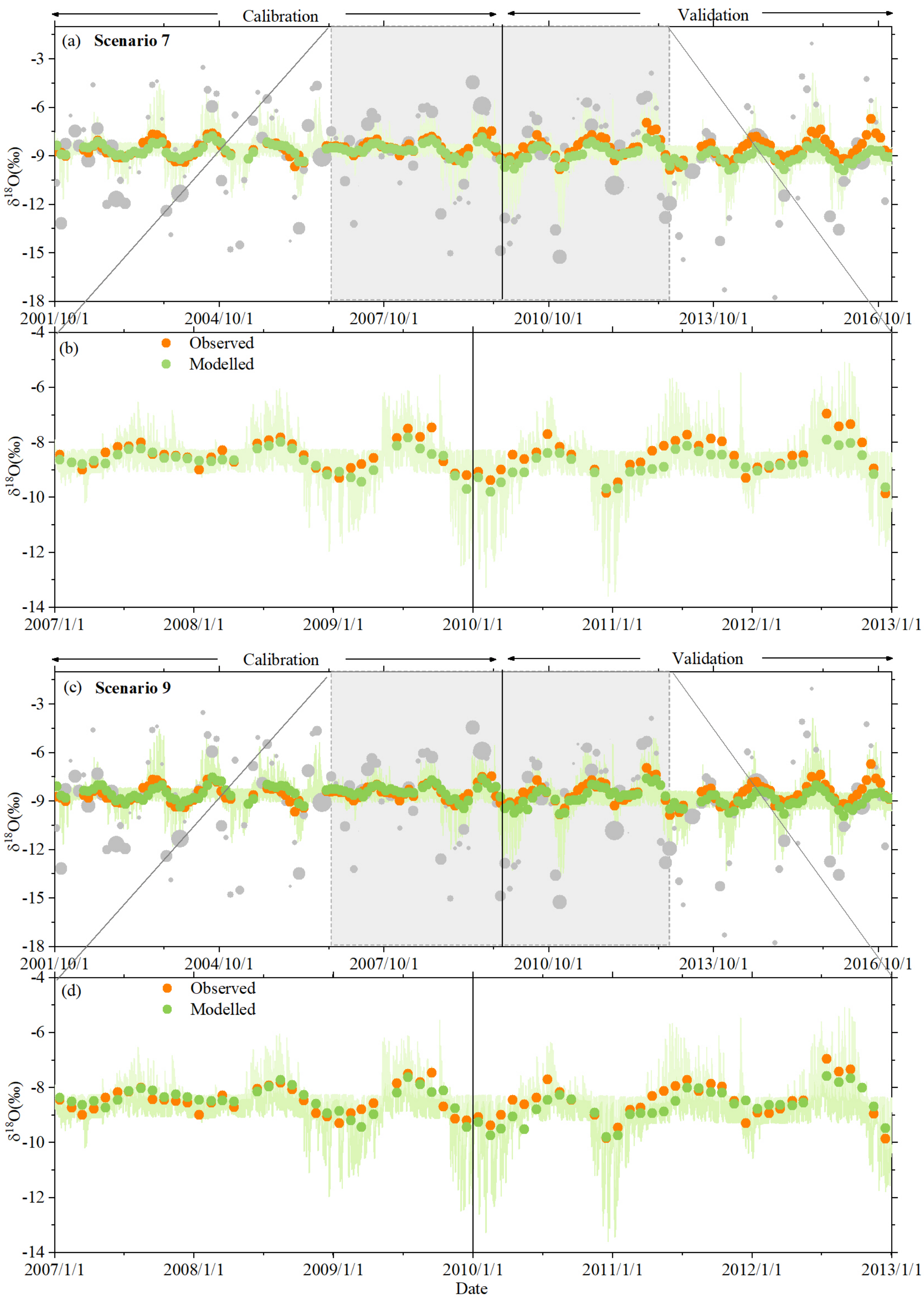

Figure S8. The time series of stream δ^{18}O reproduced by IM-SAS-L models based on simultaneous calibration to δ^{18}O and the streamflow signatures, i.e., calibration strategy $C_{\delta^{18}O,Q}$ (scenario 7) and $C_{\delta^{18}O,^{3}H,Q}$ (scenario 9), for the model calibration and evaluation periods. (a) Observed δ^{18}Osignals in precipitation (light grey dots; size of dots indicates the precipitation volume) and observed stream δ^{18}Osignals (orange dots) as well as the modelled stream δ^{18}Osignals (green dots) and the 5th/95th percentile of all retained pareto optimal solutions obtained from calibration strategy $C_{\delta^{18}O,Q}$ (light green shaded area) for scenarios 7, (b) zoom-in of observed and modelled δ^{18}O signals in the stream for the 01/01/2007 – 31 /12/2012 period for scenarios 7, (c) Observed δ^{18}Osignals in precipitation and in stream same as (a), and the modelled stream δ^{18}Osignals (relatively darker green dots) with the 5th/95th percentile of all retained pareto optimal solutions obtained from calibration strategy $C_{\delta^{18}O,^{3}H,Q}$ (light green shaded area) for scenarios 9, (d) zoom-in of observed and modelled $\delta^{18}O$ signals in the stream for the 01/01/2007 – 31/12/2012 period for scenarios 9.

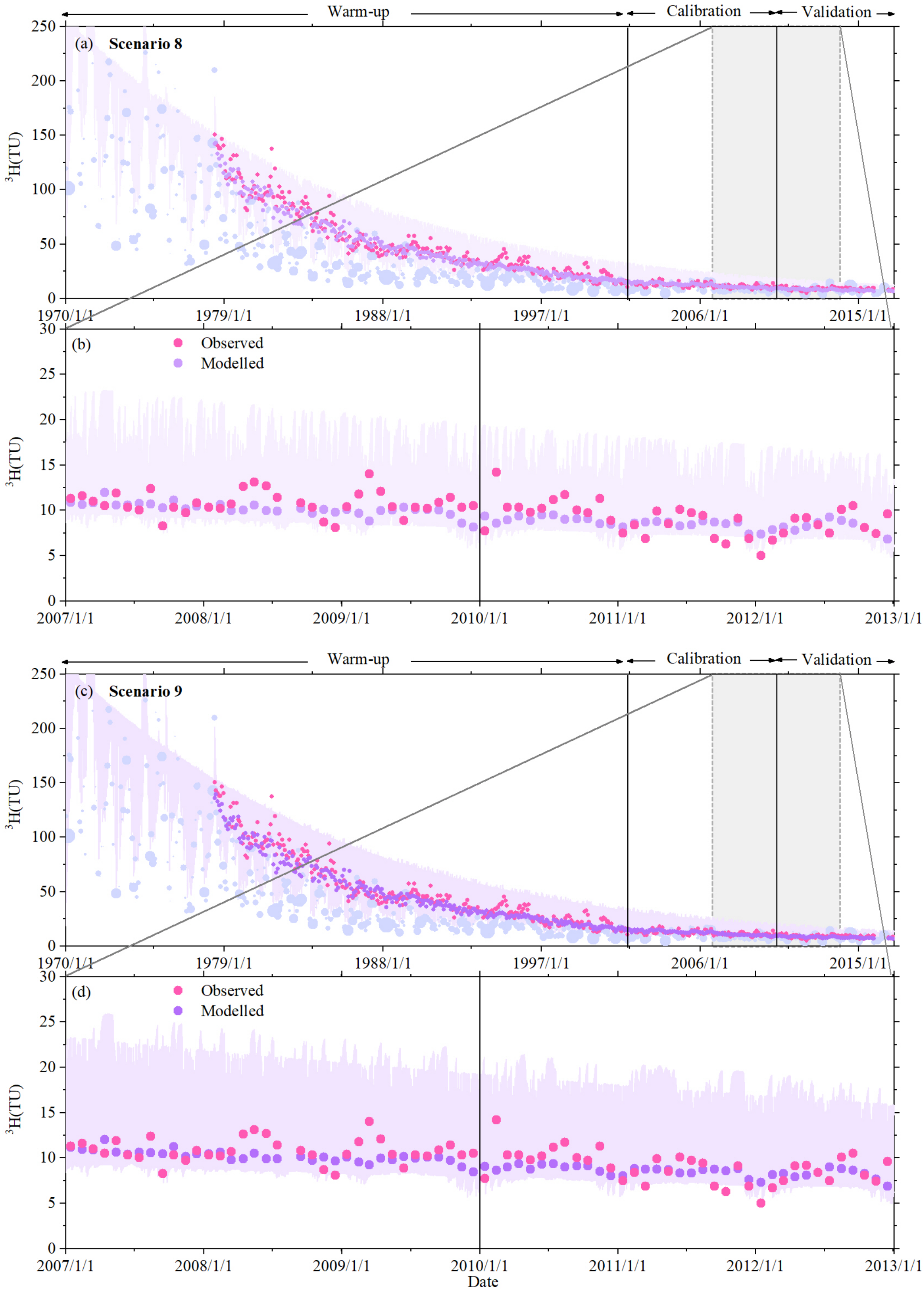

Figure S9. Time series of stream ^{3}H reproduced by model IM-SAS-L based on simultaneous calibration to tracer and the streamflow signatures, i.e. calibration strategy $C_{^{3}H,Q}$ (scenario 8) and $C_{\delta^{18}O,^{3}H,Q}$ (scenario 9), for the model calibration and evaluation periods. (a) Observed ^{3}H signals in precipitation (light blue-purple dots; size of dots indicates associated precipitation volume) and in streamflow (pink dots) as well as the modelled ^{3}H stream signal based on the most balanced solution, i.e. lowest DE (light purple dots), and the 5th/95th inter-quantile range of all retained pareto optimal solutions obtained from calibration strategy $C_{^{3}H,Q}$ (light purple shaded area) for scenario 8, (b) zoom-in of observed and modelled ^{3}H signals for the 01/01/2007 – 31/12/2012 period for scenario 8, (c) Observed ^{3}H signals in precipitation and in stream same as (a), and the modelled stream ^{3}H signals (relatively darker purple dots) and the 5th/95th percentile of all retained pareto optimal solutions obtained from calibration strategy $C_{\delta^{18}O,{}^3H,Q}$ (light purple shaded area) for scenarios 9, (d) zoom-in of observed and modelled ^{3}H signals in the stream for the 01/01/2007 – 31/12/2012 period for scenarios 9.

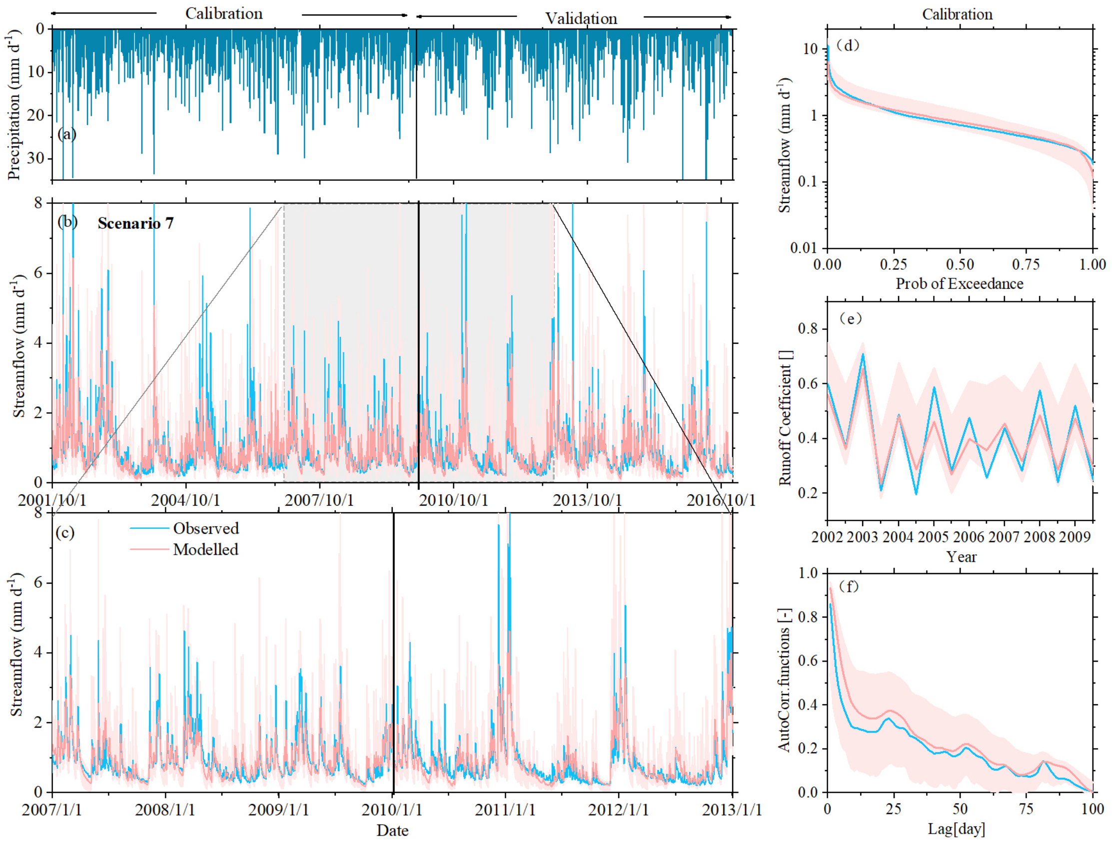

Figure S10. Hydrograph and selected hydrological signatures reproduced by IM-SAS-L, following a simultaneous calibration to the hydrological response and δ^{18}O ($C_{\delta^{18}O,Q}$; scenario 7). (a) Time series of observed daily precipitation; observed and modelled (b) daily stream flow (Q), where the light red line indicates the most balanced solution, i.e., lowest D_E, and the light red shaded area the 5th/95th inter-quantile range obtained from all pareto optimal solutions; (c) stream flow zoomed-in to the 01/01/2007 – 31/12/2012 period; (d) flow duration curves (FDC), (e) seasonal runoff coefficients (RC_Q) and (f) autocorrelation functions of stream flow (AC_Q) for the calibration period. Blue lines indicate values based on observed streamflow (Q_o), light red lines are values based on modelled stream flow (Q_m) representing the most balanced solutions, i.e., lowest D_E and the light red shaded areas show the 5th/95th inter-quantile ranges obtained from all pareto optimal solutions.

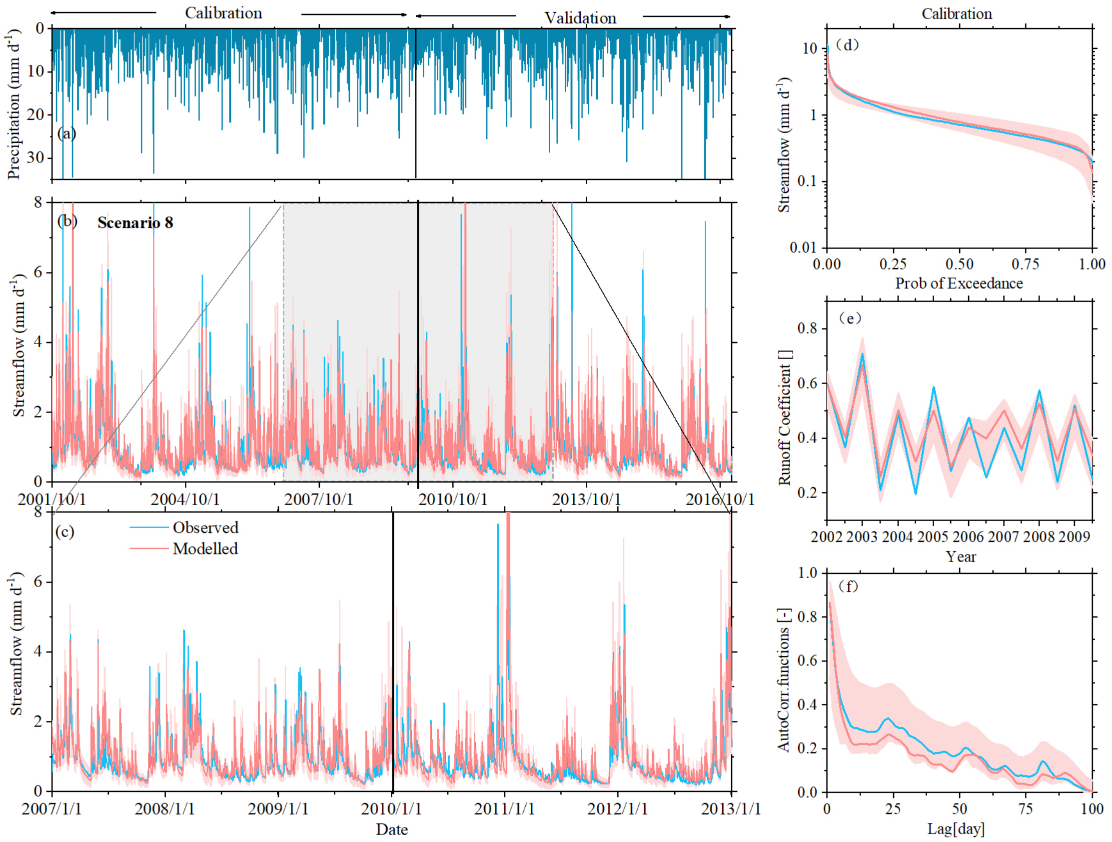

Figure S11. Hydrograph and selected hydrological signatures reproduced by IM-SAS-L, following a simultaneous calibration to the hydrological response and ^{3}H ($C^3_{H,Q}$; scenario 8). (a) Time series of observed daily precipitation; observed and modelled (b) daily stream flow (Q), where the light red line indicates the most balanced solution, i.e., lowest D_E, and the light red shaded area the 5th/95th inter-quantile range obtained from all pareto optimal solutions; (c) stream flow zoomed-in to the 01/01/2007 – 31/12/2012 period; (d) flow duration curves (FDC), (e) seasonal runoff coefficients (RC_Q) and (f) autocorrelation functions of stream flow (AC_Q) for the calibration period. Blue lines indicate values based on observed streamflow (Q_o), light red lines are values based on modelled stream flow (Q_m) representing the most balanced solutions, i.e., lowest D_E and the light red shaded areas show the 5th/95th inter-quantile ranges obtained from all pareto optimal solutions.

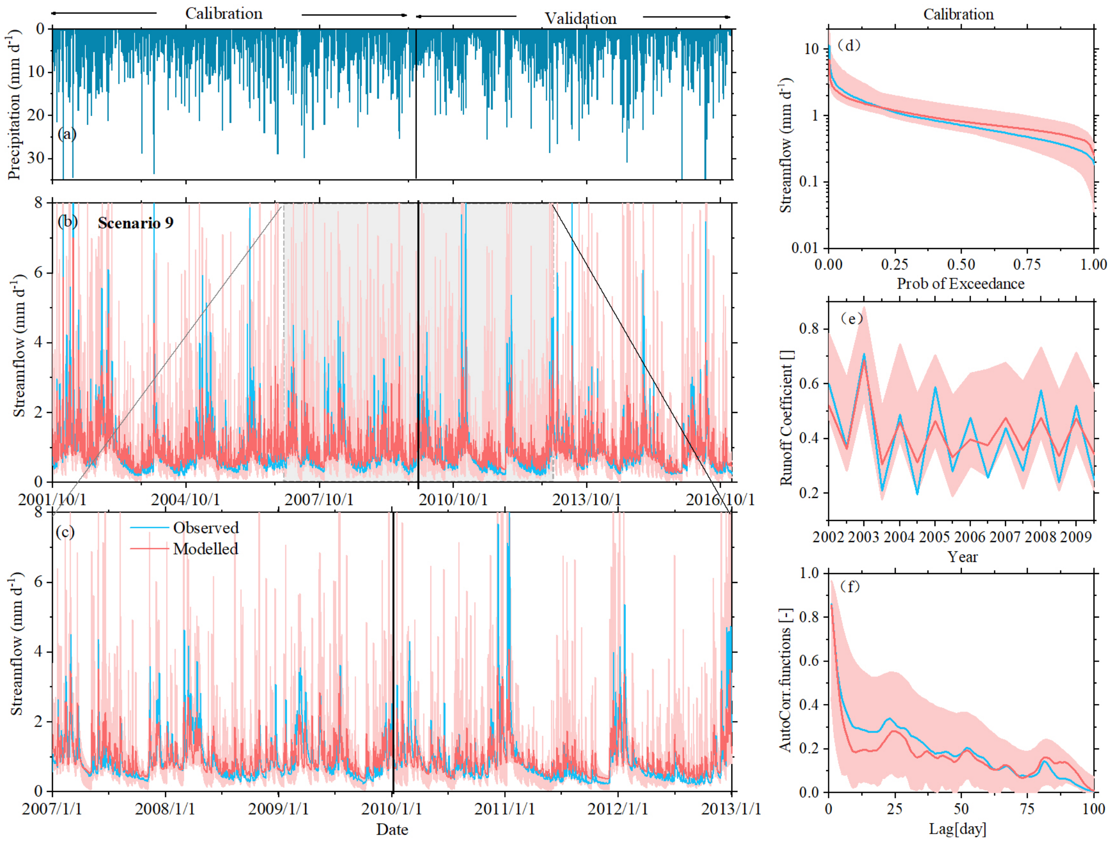

Figure S12. Hydrograph and selected hydrological signatures reproduced by IM-SAS-L, following a simultaneous calibration to the hydrological response, $\delta^{18}O$ and ^{3}H ($C_{\delta^{18}O,{}^{3}H,Q}$; scenario 9). (a) Time series of observed daily precipitation; observed and modelled (b) daily stream flow (Q), where the light red line indicates the most balanced solution, i.e., lowest D_E, and the light red shaded area the $5^{th}/95^{th}$ inter-quantile range obtained from all pareto optimal solutions; (c) stream flow zoomed-in to the 01/01/2007 – 31/12/2012 period; (d) flow duration curves (FDC), (e) seasonal runoff coefficients (RC_Q) and (f) autocorrelation functions of stream flow (AC_Q) for the calibration period. Blue lines indicate values based on observed streamflow (Q_o), light red lines are values based on modelled stream flow (Q_m) representing the most balanced solutions, i.e., lowest D_E and the light red shaded areas show the $5^{th}/95^{th}$ inter-quantile ranges obtained from all pareto optimal solutions.

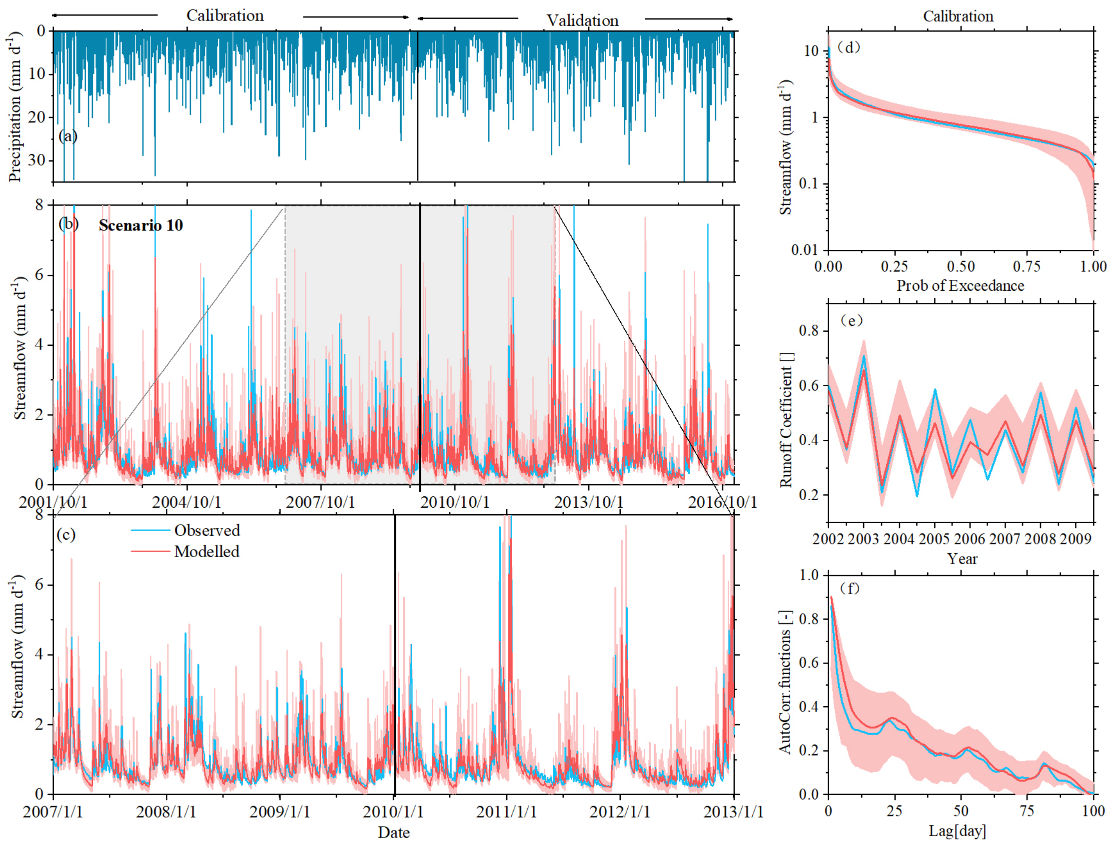

Figure S13. Hydrograph and selected hydrological signatures reproduced by IM-SAS-D, following a simultaneous calibration to the hydrological response and $\delta^{18}O$ ($C_{\delta^{18}O,Q}$; scenario 10). (a) Time series of observed daily precipitation; observed and modelled (b) daily stream flow (Q), where the light red line indicates the most balanced solution, i.e., lowest D_E, and the light red shaded area the 5th/95th inter-quantile range obtained from all pareto optimal solutions; (c) stream flow zoomed-in to the 01/01/2007 – 31/12/2012 period; (d) flow duration curves (FDC), (e) seasonal runoff coefficients (RC_Q) and (f) autocorrelation functions of stream flow (AC_Q) for the calibration period. Blue lines indicate values based on observed streamflow (Q_o), light red lines are values based on modelled stream flow (Q_m) representing the most balanced solutions, i.e., lowest D_E and the light red shaded areas show the 5th/95th inter-quantile ranges obtained from all pareto optimal solutions.

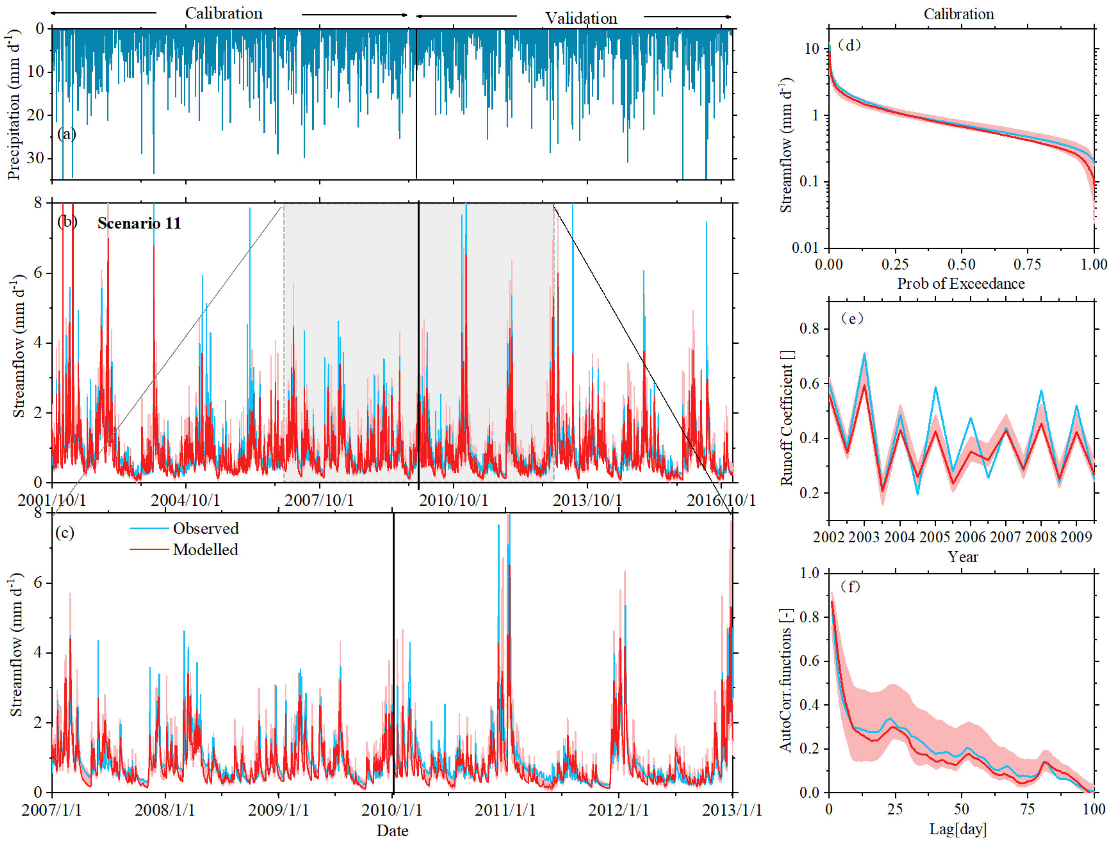

Figure S14. Hydrograph and selected hydrological signatures reproduced by IM-SAS-D, following a simultaneous calibration to the hydrological response and ^{3}H ($C^{3}_{H,Q}$; scenario 11). (a) Time series of observed daily precipitation; observed and modelled (b) daily stream flow (Q), where the red line indicates the most balanced solution, i.e., lowest D_E, and the light red shaded area the $5^{th}/95^{th}$ inter-quantile range obtained from all pareto optimal solutions; (c) stream flow zoomed-in to the 01/01/2007 – 31/12/2012 period; (d) flow duration curves (FDC), (e) seasonal runoff coefficients (RC_Q) and (f) autocorrelation functions of stream flow (AC_Q) for the calibration period. Blue lines indicate values based on observed streamflow (Q_o), red lines are values based on modelled stream flow (Q_m) representing the most balanced solutions, i.e., lowest D_E and the light red shaded areas show the $5^{th}/95^{th}$ inter-quantile ranges obtained from all pareto optimal solutions.

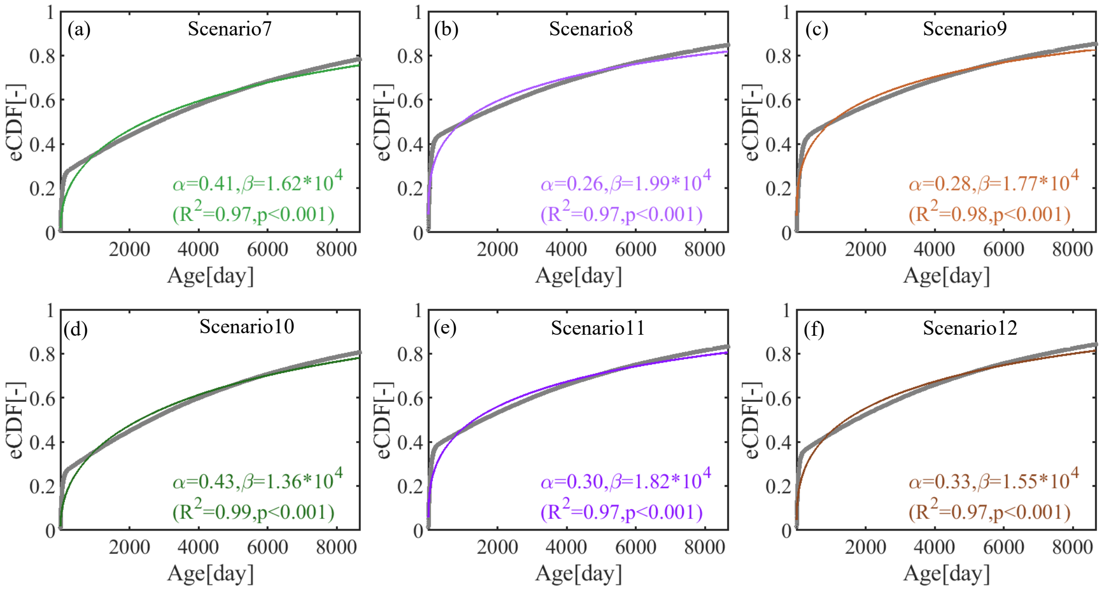

Figure S15. The Gamma distributions to the volume-weighted mean steam flow TTDs of model IM-SAS (i.e., scenarios 7-12) based on model IM-SAS-L in (a)-(c) and model IM-SAS-D in (d)-(f). Grey shades in (a)-(f) indicate volume-weighted mean TTDs and colored shades indicate the corresponding fitting Gamma distributions, respectively.

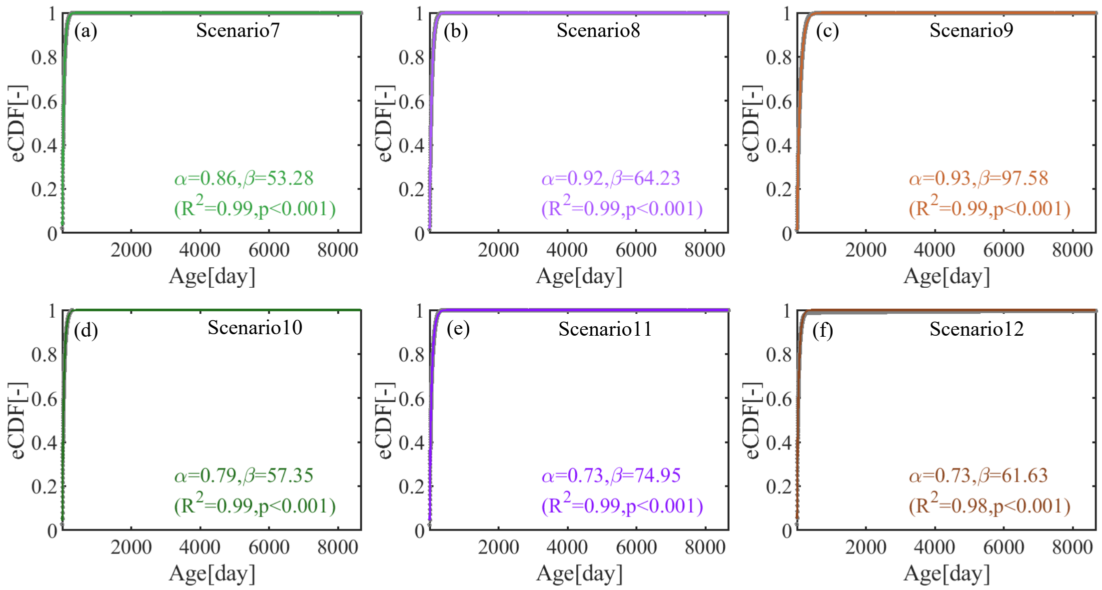

Figure S16. The Gamma distributions to the volume-weighted mean transpiration (E_a) TTDs of model IM-SAS (i.e., scenarios 7-12) based on model IM-SAS-L in (a)-(c) and model IM-SAS-D in (d)-(f). Grey shades in (a)-(f) indicate volume-weighted mean TTDs and colored shades indicate the corresponding fitting Gamma distributions, respectively.

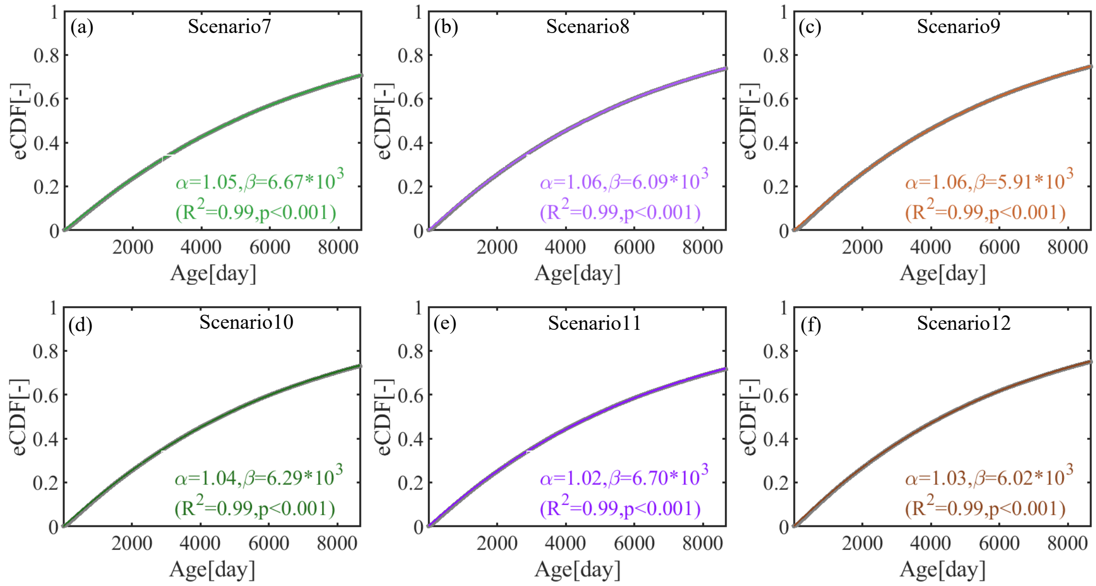

Figure S17. The Gamma distributions to the volume-weighted mean groundwater (S_s) RTDs of model IM-SAS (i.e., scenarios 7-12) based on model IM-SAS-L in (a)-(c) and model IM-SAS-D in (d)-(f). Grey shades in (a)-(f) indicate volume-weighted mean RTDs and colored shades indicate the corresponding fitting Gamma distributions, respectively.

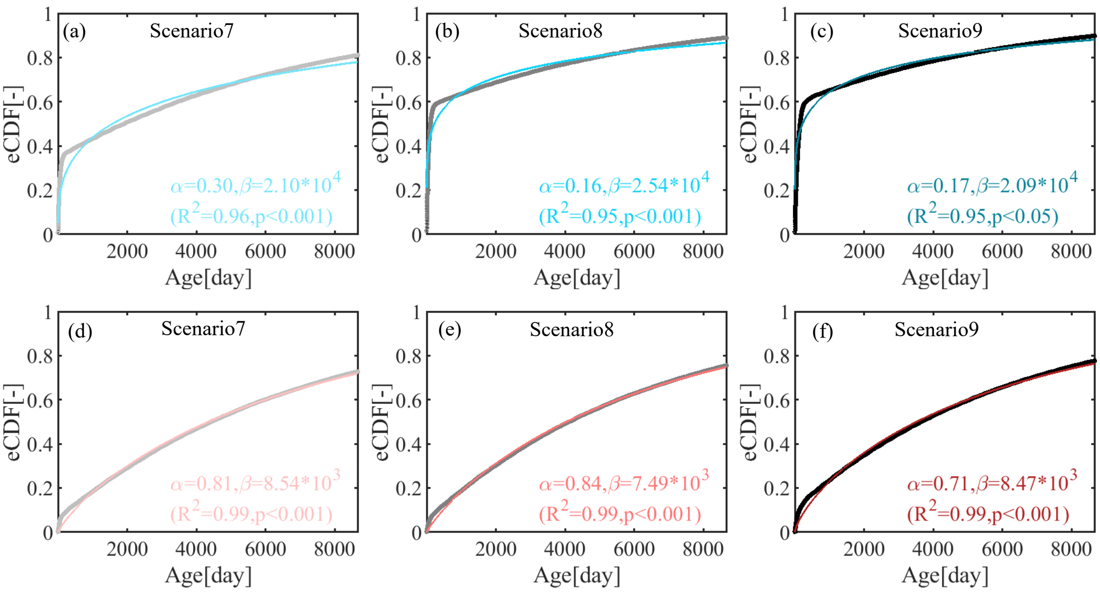

Figure S18. The Gamma distributions to the volume-weighted mean steam flow TTDs for the wet and dry periods of model IM-SAS-L (i.e., scenarios 7-9) based on wet periods in (a)-(c) and dry periods in (d)-(f). Grey shade and blue shades in (a)-(c) indicate volume-weighted mean TTDs for wet periods and the corresponding fitting Gamma distributions, respectively; grey shade and red shades in (d)-(f) indicate volume-weighted mean TTDs for dry periods and the corresponding fitting Gamma distributions, respectively.

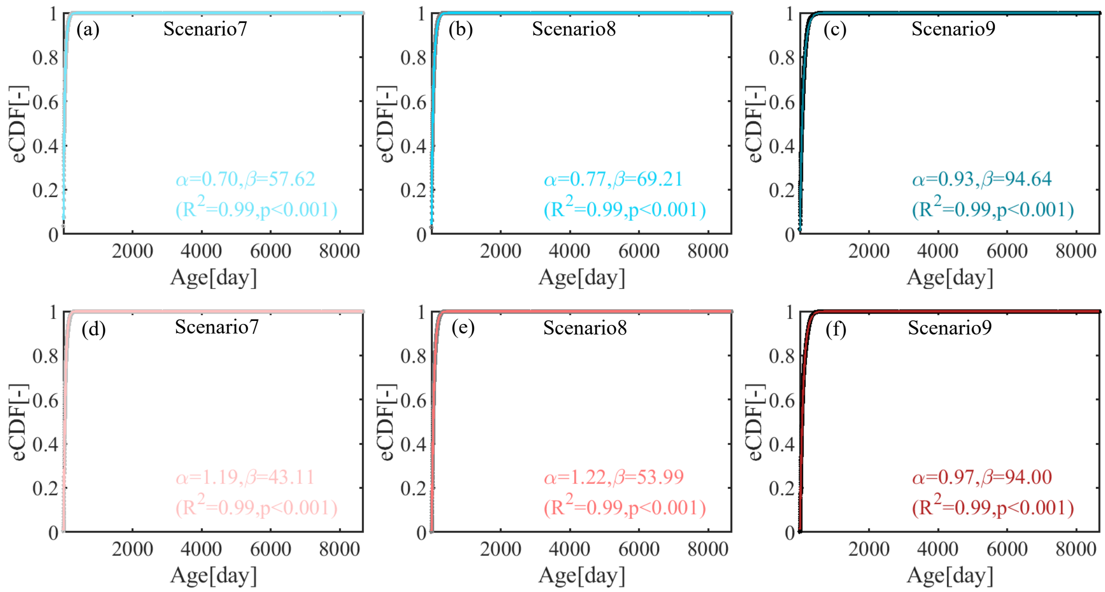

Figure S19. The Gamma distributions to the volume-weighted mean transpiration (E_a) TTDs for the wet and dry periods of model IM-SAS-L (i.e., scenarios 7-9) based on wet periods in (a)-(c) and dry periods in (d)-(f). Grey shade and blue shades in (a)-(c) indicate volume-weighted mean TTDs for wet periods and the corresponding fitting Gamma distributions, respectively; grey shade and red shades in (d)-(f) indicate volume-weighted mean TTDs for dry periods and the corresponding fitting Gamma distributions, respectively.

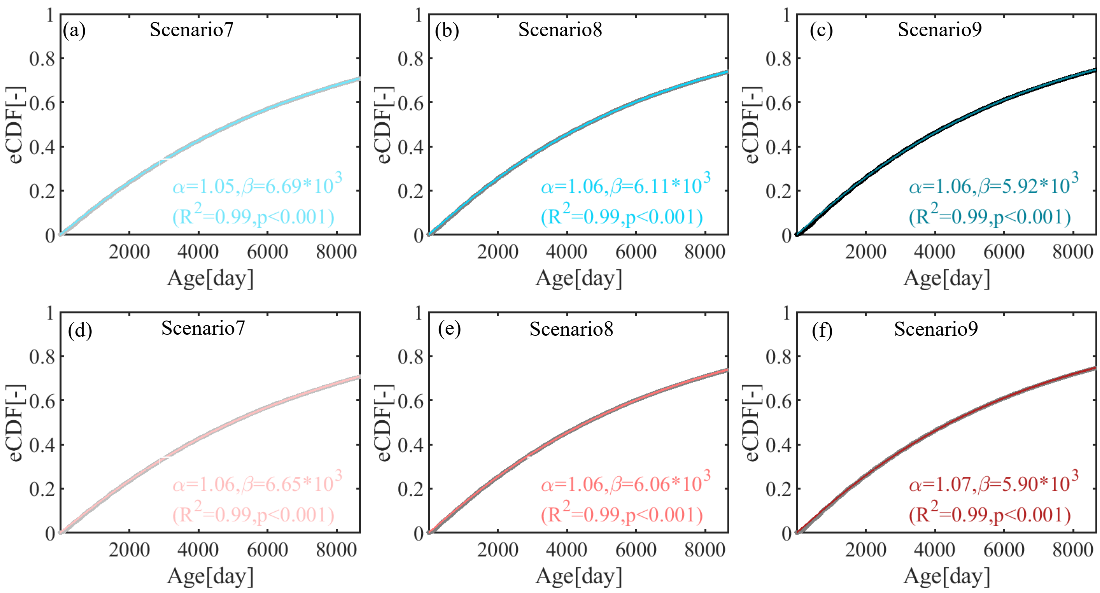

Figure S20. The Gamma distributions to the volume-weighted mean groundwater (S_s) RTDs for the wet and dry periods of model IM-SAS-L (i.e., scenarios 7-9) based on wet periods in (a)-(c) and dry periods in (d)-(f). Grey shade and blue shades in (a)-(c) indicate volume-weighted mean RTDs for wet periods and the corresponding fitting Gamma distributions, respectively; grey shade and red shades in (d)-(f) indicate volume-weighted mean RTDs for dry periods and the corresponding fitting Gamma distributions, respectively.

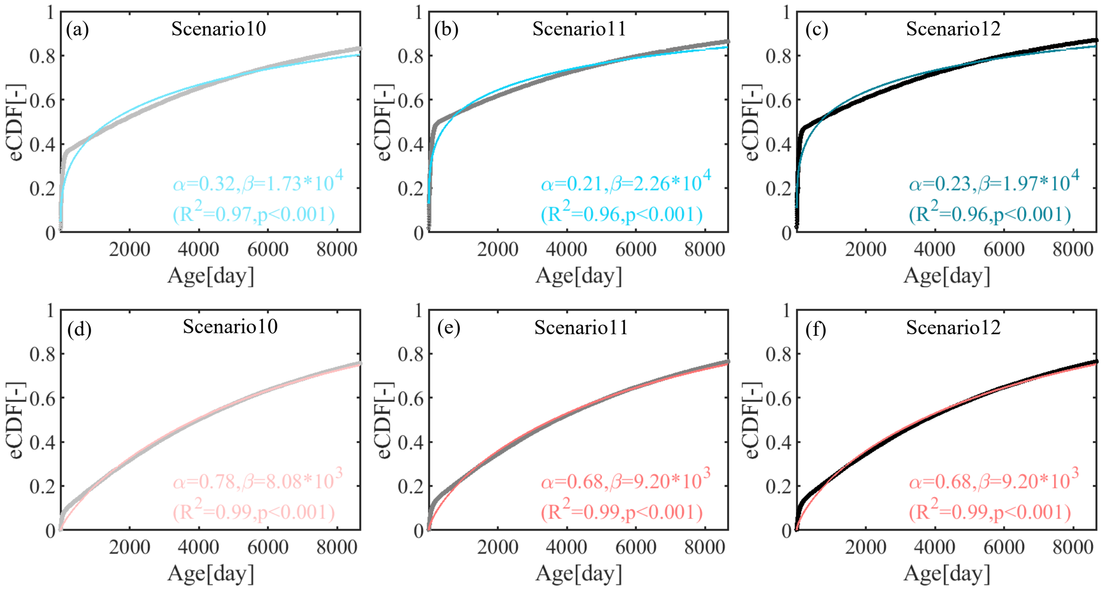

Figure S21. The Gamma distributions to the volume-weighted mean steam flow TTDs for the wet and dry periods of model IM-SAS-D (i.e., scenarios 10-12) based on wet periods in (a)-(c) and dry periods in (d)-(f). Grey shade and blue shades in (a)-(c) indicate volume-weighted mean TTDs for wet periods and the corresponding fitting Gamma distributions, respectively; grey shade and red shades in (d)-(f) indicate volume-weighted mean TTDs for dry periods and the corresponding fitting Gamma distributions, respectively.

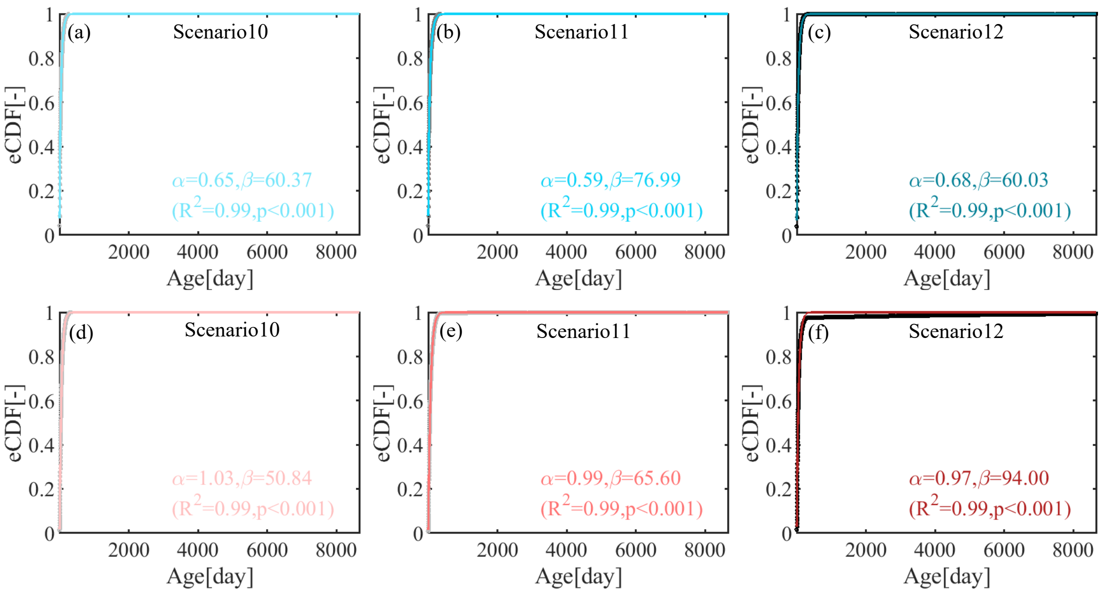

Figure S22. The Gamma distributions to the volume-weighted mean transpiration (E_a) TTDs for the wet and dry periods of model IM-SAS-D (i.e., scenarios 10-12) based on wet periods in (a)-(c) and dry periods in (d)-(f). Grey shade and blue shades in (a)-(c) indicate volume-weighted mean TTDs for wet periods and the corresponding fitting Gamma distributions, respectively; grey shade and red shades in (d)-(f) indicate volume-weighted mean TTDs for dry periods and the corresponding fitting Gamma distributions, respectively.

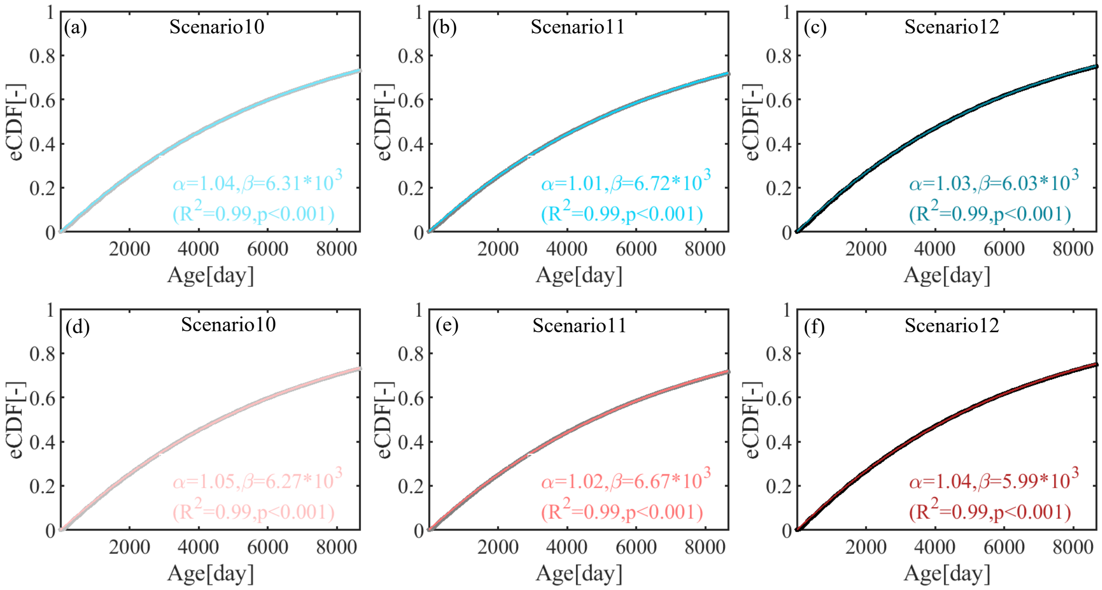

Figure S23. The Gamma distributions to the volume-weighted mean groundwater (S_s) RTDs for the wet and dry periods of model IM-SAS-D (i.e., scenarios 10-12) based on wet periods in (a)-(c) and dry periods in (d)-(f). Grey shade and blue shades in (a)-(c) indicate volume-weighted mean RTDs for wet periods and the corresponding fitting Gamma distributions, respectively; grey shade and red shades in (d)-(f) indicate volume-weighted mean RTDs for dry periods and the corresponding fitting Gamma distributions, respectively.

Table S3. Water balance and constitutive equations of distributed hydrological model

Reservoirs	Water balance		Constitutive equations	
Interception	$\frac{ds_i}{dt} = P_{rain} - E_i - P_{re}$	(S4)	$P_{rain} = P, when\, T > T_t$	(S10)
			$E_i = \min(E_p, S_i/dt)$	(S11)
			$P_{re} = \max((S_i - S_{imax})/dt, 0)$	(S12)
Snow	$\frac{ds_{snow}}{dt} = P_{snow} - M_{snow}$	(S5)	$P_{snow,e} = P, when\, T_e \leq T_t$	(S13)
			$P_{snow} = \sum P_{snow,e} \cdot W_e$	(S14)
			$M_{snow,e} = \min(C_{melt} * (T_e - T_t), S_{snow,e}/dt), when\, T_e > T_t$	(S15)
			$M_{snow} = \sum M_{snow,e} \cdot W_e$	(S16)
Unsaturated reservoir	Forest/ Grass: $\frac{ds_u}{dt} = P_e - E_a - R_u - R_{perc}$	(S6)	$P_e = P_{re} + M_{snow}$	(S17)
			$\rho = S_u/S_{umax}$	(S18)
			$E_a = (E_p - E_i) * \min(\rho/C_a, 1)$	(S19)
			$C_r = 1 - (1 - \rho)^{\gamma}$	(S20)
	Wetland: $\frac{ds_u}{dt} = P_e - E_a - R_u + R_{cap}$	(S7)	$R_u = (1 - C_r) * P_e$	(S21)
			$R_{perc} = \min\,(c_{pmax} * \rho, S_u/dt)$	(S22)
			$R_{cap} = \min\,(c_{pmax} * (1 - \rho), \frac{S_s}{dt} * P_{HRU})$	(S23)
			$R_{pref} = (1 - D) * R_u$	(S24)
Fast reservoir	$\frac{ds_f}{dt} = R_f - Q_f$	(S8)	Forest/ Grass: $R_f = D * R_u$	(S25)
			Wetland: $R_f = R_u$	(S26)
			$Q_f = K_f * S_f$	(S27)
Slow reservoir	$\frac{ds_s}{dt} = R_{perctot} + R_{preftot} - R_{captot} - Q_s$	(S9)	$R_{perctot} = \sum R_{perc} \cdot P_{HRU}$	(S28)
			$R_{preftot} = \sum R_{pref} \cdot P_{HRU}$	(S29)
			$R_{captot} = \sum R_{cap} \cdot P_{HRU}$	(S30)
			$Q_s = K_s * S_s$	(S31)

Table S4. Model parameters and their prior ranges and constraints in Borg_MOEA method.

	Parameters	Unit	Description	Parameter Constraints	References
Global	T_t	°C	Threshold temperature to split snowfall and rainfall		(Gao et al., 2014; M. Hrachowitz1 et al., 2013)
	C_{melt}	mm °C^{-1}	Melt factor		(D. Prenner et al.,2018)
	C_a	-	Evapotranspiration coefficient		(Gao et al., 2017)
	K_s	d^{-1}	Recession coefficient of slow response reservoir		(D. Prenner et al.,2018)
	Ssp	mm	Passive storage Volume		(Hrachowitz1 et al., 2021)
Forest	S_{imaxF}	mm	Interception capacity	S_{imaxF}>S_{imaxG}	(Gao et al., 2014)
	S_{umaxF}	mm	Root zone storage capacity	S_{umaxF}>S_{umaxG}	(Gao et al., 2014)
	γ_F	-	Shape parameter		(Gao et al., 2014)
	D	-	Splitter to fast and slow response reservoirs		(Gao et al., 2014)
	c_{pmaxF}	mm d^{-1}	Percolation capacity		(D. Prenner et al.,2018)
	K_{fF}	d^{-1}	Recession coefficient of fast response reservoir	K_{fF}>K_s	(Hrachowitz1 et al., 2013)
Grassland	S_{imaxG}	mm	Interception capacity		(Gao et al., 2014)
	S_{umaxG}	mm	Root zone storage capacity	S_{umaxG}>S_{umaxW}	(Gao et al., 2014)
	γ_G	-	Shape parameter		(Gao et al., 2014)
	c_{pmaxG}	mm d^{-1}	Percolation capacity		(D. Prenner et al.,2018)
	K_{fG}	d^{-1}	Recession coefficient of fast response reservoir	K_{fG}>K_s	(Hrachowitz1 et al., 2013)
Wetland	S_{umaxW}	mm	Root zone storage capacity	$S_{umaxW} < S_{umaxG}$	(Gao et al., 2014)
	γ_W	-	Shape parameter		(Gao et al., 2014)
	c_{rmax}	mm d^{-1}	Percolation capacity		(Gao et al., 2014)
	K_{fW}	d^{-1}	Recession coefficient of fast response reservoir	K_{fW}>K_s	(D. Prenner et al.,2018)

Table S5. Performance metrics of the model implementations and the associated calibration strategies for the 2001 – 2009 calibration period (cal.) and the 2010 – 2016 model evaluation period (val.). The ranges of all performance metrics for the full set of pareto optimal solutions for the multi-objective calibration cases (Scenarios 7 – 12) are shown here.

Scenario			7	8	9	10	11	12
Model				IM-SAS-L			IM-SAS-D	
Implementation				Lumped			Distributed	
Calibration strategy → Performance metric ↓			$C_{\delta^{18}O,Q}$	$C_{^3H,Q}$	$C_{\delta^{18}O,^3H,Q}$	$C_{\delta^{18}O,Q}$	$C_{^3H,Q}$	$C_{\delta^{18}O,^3H,Q}$
Performance metrics	$MSE_{\delta^{18}O}$	cal.	0.070-0.347	-	0.068-0.756	0.068-0.188	-	0.068-0.262
		val.	0.134-0.733	-	0.116-1.006	0.129-0.648	-	0.141-0.905
	$MSE_{^3H}$	cal.	-	2.972-71.69	2.823-130.6	-	2.956-19.75	2.975-47.54
		val.	-	1.825-19.97	1.908-40.46	-	1.932-4.883	1.915-13.29
	MSE_Q	cal.	0.194-1.287	0.193-0.703	0.196-2.762	0.228-0.817	0.232-0.442	0.248-1.161
		val.	0.211-1.239	0.212-0.706	0.215-2.572	0.251-0.827	0.253-0.454	0.273-1.118
	$MSE_{log(Q)}$	cal.	0.090-0.584	0.091-0.304	0.098-0.621	0.119-0.334	0.101-0.231	0.112-0.399
		val.	0.088-0.662	0.080-0.362	0.083-0.582	0.101-0.321	0.088-0.310	0.105-0.485
	MSE_{FDC_Q}	cal.	0.003-0.359	0.003-0.129	0.003-1.042	0.002-0.144	0.002-0.072	0.002-0.212
		val.	0.004-0.369	0.002-0.195	0.007-0.877	0.003-0.141	0.012-0.111	0.004-0.180
	$MSE_{FDC_{log(Q)}}$	cal.	0.001-0.173	0.002-0.126	0.002-0.377	0.002-0.119	0.002-0.051	0.002-0.167
		val.	0.003-0.229	0.002-0.207	0.003-0.345	0.002-0.093	0.004-0.127	0.003-0.251
	MSE_{RC}	cal.	0.003-0.045	0.003-0.011	0.003-0.070	0.003-0.018	0.002-0.006	0.002-0.026
		val.	0.003-0.040	0.002-0.011	0.002-0.064	0.002-0.016	0.002-0.008	0.002-0.023
	MSE_{AC_Q}	cal.	0.000-0.030	0.000-0.019	0.000-0.034	0.000-0.013	0.000-0.016	0.000-0.019
		val.	0.000-0.034	0.000-0.026	0.000-0.045	0.000-0.027	0.000-0.019	0.000-0.031